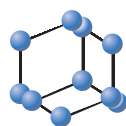


## RESEARCH ARTICLE

# Theoretical Studies on the Selectivity Mechanisms of Glycogen Synthase Kinase 3 $\beta$ (GSK3 $\beta$ ) with Pyrazine ATP-competitive Inhibitors by 3D-QSAR, Molecular Docking, Molecular Dynamics Simulation and Free Energy Calculations



**BENTHAM  
SCIENCE**

Jingyu Zhu<sup>1,#,\*</sup>, Yuanqing Wu<sup>1,#</sup>, Lei Xu<sup>2</sup> and Jian Jin<sup>1,\*</sup>

<sup>1</sup>School of Pharmaceutical Sciences, Jiangnan University, Wuxi, Jiangsu 214122, P.R. China; <sup>2</sup>Institute of Bioinformatics and Medical Engineering, School of Electrical and Information Engineering, Jiangsu University of Technology, Changzhou 213001, P.R. China

**Abstract: Background:** Glycogen synthase kinase-3 (GSK3) is associated with various key biological processes and has been considered as an important therapeutic target for the treatment of many diseases. Great efforts have been made on the development of GSK3 inhibitors, especially ATP-competitive GSK3 $\beta$  inhibitor, but it is still a great challenge to develop selective GSK3 $\beta$  inhibitors because of the high sequence homology with other kinases.

**Objective:** In order to reveal the selectivity mechanisms of GSK3 $\beta$  inhibition at the molecular level, a series of ATP-competitive GSK3 $\beta$  inhibitor was analyzed by a systematic computational method, combining 3D-QSAR, molecular docking, molecular dynamic simulations and free energy calculations.

**Methods:** Firstly, 3D-QSAR with CoMFA was built to explore the general structure activity relationships. Secondly, CDOCKER and Flexible docking were employed to predicted the reasonable docking poses of all studied inhibitors. And then, both GSK3 $\beta$  and CDK2 complexes were selected to conduct molecular dynamics simulations. Finally, the free energy calculations were employed to find the key selective-residues.

**Results:** CoMFA model suggested the steric, hydrophobic fields play key roles in the bioactivities of inhibitors, and the binding mechanisms were well analyzed through molecular docking. The binding free energies predicted are in good agreement with the experimental bioactivities and the free energy calculations showed that the binding of GSK3 $\beta$ /inhibitors was mainly contributed from hydrogen bonding and hydrophobic interaction.

**Conclusion:** Some key residues for selective binding were highlighted, which may afford important guidance for the rational design of novel ATP-competitive GSK3 $\beta$  inhibitors.

## ARTICLE HISTORY

Received: March 23, 2019  
Revised: May 16, 2019  
Accepted: June 09, 2019

DOI:  
10.2174/1573409915666190708102459



CrossMark

**Keywords:** GSK3 $\beta$  ATP-competitive inhibitors, selective inhibitors, 3D-QSAR CoMFA, molecular docking, molecular dynamics simulation, free energy calculation.

## 1. INTRODUCTION

Glycogen synthase kinase-3 (GSK3) is a ubiquitously expressed serine/threonine protein kinase implicated in the regulation of many physiological responses in mammalian cells by phosphorylating a variety of cytoplasmic and nuclear proteins, that modulates many fundamental signaling pathways including processes of glucose metabolism, Wnt signaling, abnormal excessive phosphorylation of tau protein

etc. [1, 2]. Moreover, the kinase GSK3 can be divided into GSK3 $\alpha$  and GSK3 $\beta$ , which is inhibited by external phosphorylation of Ser<sup>21</sup> in  $\alpha$  isoform and Ser<sup>9</sup> in  $\beta$ , respectively [3]. Since GSK3 has multifaceted roles in many signaling pathways, an elevation or relegation of its normal activity level is associated with several diseases, such as type-2 diabetes and Alzheimer's disease. GSK3 has recently emerged as a potential therapeutic target [4-10].

In the past decades, GSK3 $\beta$  has received more attention and a number of GSK3 $\beta$  inhibitors have been designed and reported successively, and these inhibitors are mainly divided into two types: ATP competition and non-ATP competition inhibitors [11-14]. In the last couple years, significant effort has been devoted to the development of ATP competi-

\*Address correspondence to these authors at the School of Pharmaceutical Sciences, Jiangnan University, Wuxi, Jiangsu 214122, P.R. China; Tel: (+86)-15850181870; Emails: [jingyuzhu@jiangnan.edu.cn](mailto:jingyuzhu@jiangnan.edu.cn); [jianjin@jiangnan.edu.cn](mailto:jianjin@jiangnan.edu.cn)

#These authors contributed equally to this work

tion GSK3 $\beta$  inhibitors, but so far, none of these inhibitors have advanced to clinical trials. There could be two reasons for this failure [15]: On the one hand, the two isoforms of GSK3 show 97% identical in sequence within the catalytic domain [11]; on the other hand, most ATP competitive GSK3 $\beta$  inhibitors potentially inhibit other kinases, especially CDK2 (Cyclin-dependent kinase) [11, 16, 17]. Therefore, it would be a great challenge to develop specific GSK3 $\beta$  inhibitors. Compared with traditional structure-activity relationship studies, computer-aided drug design (CADD) methods may provide systematic investigations on the selective GSK3 $\beta$  binding mechanism of the ATP competitive inhibitors at the molecular level [18-24]. As an important technology and tool for drug design, CADD, including quantitative structure-activity relationship (QSAR) analysis, molecular docking, molecular dynamics (MD) simulation and free energy calculations *etc.*, has been widely used to design or discover novel GSK3 $\beta$  inhibitors [19, 25-27]. But the theoretical studies on the selectivity mechanisms of GSK3 $\beta$  through these simulation techniques are quite limited. Therefore in this study, a computational strategy, which combined 3D-QSAR, molecular docking, MD simulation, free energy calculations and decomposition, was employed to reveal the mechanisms of GSK3 $\beta$  binding selectivity. Our findings may provide some useful enlightenment for the development of high selective GSK3 $\beta$  inhibitors.

## 2. MATERIALS AND METHODS

### 2.1. 3D-QSAR

#### 2.1.1. Data Set

Thirty-one compounds were selected for the generation of CoMFA model based on the GSK3 $\beta$  inhibitory activity as reported (Table 1) [28]. Based on the diversity and activity range of molecular structure, the whole data set was divided into training set containing 24 compounds for 3D-QSAR model generation and testing set containing 7 compounds for model checking through the *Generate Training and Test Data* module of Discovery Studio 3.5 (DS3.5). In this process, *Split* method is modified to *random*, and the ratio of the training set to the test set is approximately 3:1. All the inhibitors were sketched by sybyl-x2.0, and the energy minimization procedure was used in sybyl-x2.0 to achieve stable conformations and the parameters were set as follows: all molecular charges using *Tripos* force field loading *Pullman* method, and the biggest iterations were set to 10000, *energy gradient* will be limited to 0.005 kcal/(mol·Å), other parameters as the default values. The related IC<sub>50</sub> values were converted to PIC<sub>50</sub> values (-log IC<sub>50</sub>) as the response variable for QSAR studies, the structures and PIC<sub>50</sub> experimental values of all compounds are shown in Table 1 (the test set molecules labeled with asterisk). Then, two alignment protocols were respectively built: the first approach was based on the guidelines provided by Sybyl, the compounds of the training and test sets were superimposed with the common skeleton [21] (Fig. S1a) of the Cpd25, which was selected as the template molecule with the highest active, and the superimposed model is shown in Fig. S1b; another approach was based on the conformational poses from molecular docking, and the superimposed model is shown in Fig. (S2f).

### 2.1.2. CoMFA Model Building

In the CoMFA analyses, the following CoMFA fields were evaluated: traditional steric and electrostatic fields, H-bond donor and acceptor fields, indicator steric and electrostatic fields. Partial least squared (PLS), which is a kind of multiple linear regression, was used to construct a 3D-QSAR model with the link between the biological activity and molecular description. In order to get a more accurate and test the reliability of the model, then leave-one-out (LOO) cross-validation method was adopted to get the statistical parameters including conventional correlation coefficient ( $r^2$ ), standard error of estimate (SEE) and F-test values, the optimum principal component number (N) and the coefficient of cross validation ( $q^2$ ). When the  $q^2 > 0.5$ ,  $r^2 > 0.9$ , the model has significant statistical criteria (other related values, F value  $> 100$ , SEE as small as possible). After internal validation, the test set was used for external validation to evaluate the ability of model prediction. Subsequently, the biological activities of test set compounds were predicted by the CoMFA mode and the predictive ability was expressed by the predictive correlation coefficient ( $R^2_{test}$ ).

## 2.2. Molecular Docking

### 2.2.1. Preparation of Inhibitors and Protein

The four crystal structures of GSK3 $\beta$  (PDB entry: 4ACC, 4ACD, 4ACG, 4ACH) [28] were used as the initial receptor for molecular docking protocol. Preparation of protein macromolecules and small ligands is required before molecular docking. First, the protein was prepared by the *prepare protein* module in DS3.5 with the default parameter, the prepared proteins would be added polar hydrogen, removed water molecules, repaired the broken chain and added the *CHARMm* field. And then, all inhibitors were processed using the *prepare ligands* module in DS3.5 all ligands were protonated and generated a series of conformations to facilitate better docking.

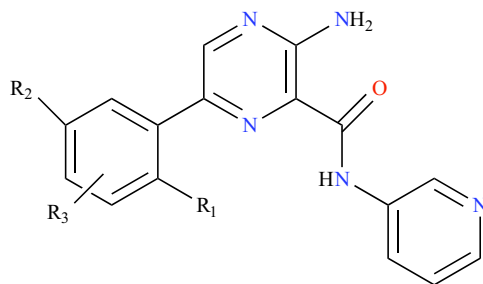
### 2.2.2. Setting of Molecular Docking Parameters

Two docking protocols, CDOCKER (CD) and Flexible docking (FD), were employed to predict the binding mode between GSK3 $\beta$  and the inhibitors. CD, a semi-flexible docking, is a relatively accurate docking method. In this process, *Top Hits* are modified to 10, and *Use Full potential* is modified to False, as well as the default active pocket radius and the active pocket radius of 5 Å size. FD is a flexible docking method and allows greater realism than other docking formalisms in that flexibility of the ligand and receptor side-chains is permitted during the docking procedure. In FD study, the amino acids in the range of 4 Å around the original ligand were defined as active residues, and then, the *Maximum Number of Generate protein conformations* was set to 100, the *Generate Ligand Conformation* method was set as fast and the *Max Hits to save* was set to 3. The remaining parameters were set as default.

## 2.3. Molecular Dynamics Simulation

Four complexes (PDB: 4ACC, 4ACG, 4ACH, 4ACM) [28] were used as the initial structures of MD simulation by

**Table 1.** The structures and experimental activities of GSK3β inhibitors. (Positions other than para substitution of R<sub>3</sub> are indicated explicitly in the table by ortho or meta, Where the R<sub>3</sub> group of the Cpd8 is in the meta position of R<sub>2</sub>, the R<sub>3</sub> group of Cpd9 is in the ortho position of R<sub>2</sub>).



No.	R <sub>1</sub>	R <sub>2</sub>	R <sub>3</sub>	IC <sub>50</sub> (nm)	PIC <sub>50</sub>
5	H	H	H	41	7.387
8	H	H	 meta	74	7.131
9	H	H	 ortho	300	6.523
10	F	H	 para	1.3	9.114
11	CH <sub>3</sub>	H	 para	0.46	9.337
12	CF <sub>3</sub>	H	 para	1.1	8.959
13	CH <sub>3</sub>	CH <sub>3</sub>	 para	1.5	8.824
14	H	F	 para	9	8.046
15	H	CH <sub>3</sub>	 para	6.3	8.201
16	H	H		2	8.699
*17	H	H		18	7.745
*18	H	H	 para	4.9	8.31

No.	R <sub>1</sub>	R <sub>2</sub>	R <sub>3</sub>	IC <sub>50</sub> /(nm)	PIC <sub>50</sub>
*19	H	H		4.4	8.357
20	H	H		0.4	9.398
21	H	H		12	7.921
22	H	H		0.67	9.174
*23	H	H		20	7.699
*24	H	H		8.4	8.076
37	H	H		3.1	8.509
38	H	H		16	7.796
<p>Core 2</p>					
No.	R	X	Y	IC <sub>50</sub> /(nm)	PIC <sub>50</sub>
27	NH <sub>2</sub>	C	C	120	6.921
28	NH <sub>2</sub>	N	C	64	7.194
41	H	N	N	370	6.432
<p>Core 3</p>					

Table 1. Contd...

No.	R <sub>3</sub>	R <sub>5</sub>	IC <sub>50</sub> /(nm)	PIC <sub>50</sub>
25			0.22	9.658
26			0.48	9.319
44			12	7.921
45			690	6.161
46			0.99	9.004
49			74	7.131
*50			90	7.046
*51			22	7.658

\* The test set molecules.

the *SANDER* program in Amber14 [29]. Then, the general Amber force field (*gaff*) [30] was used for the ligands and the Amber *ff03* force field [31] was used for the proteins. The semi-empirical *AM1* method in GAUSSIAN09 [32] was used to optimize small molecule inhibitors, partial of the atomic charge is obtained by using the RESP (restrained electrostatic potential) fitting technique to calculate the electrostatic potential at the HF/6-31G\* level. The *tleap* module in AMBER14 was used to generate the topological structure and parameter files of the proteins and ligands studied. Each system was neutralized with Na<sup>+</sup> ions, meanwhile, immersed in a rectangular box filled with *TIP3P* water molecules at a distance of 10 Å from any solute atom. The Particle Mesh Ewald (PME) scheme was used to deal with the long range electrostatics, in the range of 10 Å for van der Waals interactions.

Before the MD simulation, there are three steps to minimize the energy of each system using the *SANDER* program [33, 34]. First of all, under the condition of the principal carbon constraint (50 kcal/mol/Å<sup>2</sup>), 1000 minimization cycles (500 fastest descent cycles and 500 conjugate gradients) were performed. Secondly, 1000 cycles of minimizations with a weaker harmonic potential (10 kcal/mol/Å<sup>2</sup>) were carried out. Finally, in the absence of any constraints, the

entire system is covered by 5000 minimum cycles (1000 steepest descent cycles and 4000 conjugate gradient cycles). During the MD simulation stage, each system is gradually heated gradually from 0 to 300K over 50 ps in the NPT ensemble. and then performed a 50-ps MD simulation in NPT ensemble with a temperature of 300 K and pressure 1 atm. At last, a 30 ns NPT MD simulation was performed, using the *SHAKE* algorithm to bind all the bonds involving hydrogen and the time step was set to 2.0 fs. Coordinates were saved every 10 ps [35].

#### 2.4. MM/GBSA Free Energy Calculations and Decomposition

Each system is the combination of free energy calculation ( $\Delta G_{\text{bind}}$ ) by MM/GBSA method, the following Equation (1) [36-39].

$$\begin{aligned} \Delta G_{\text{bind}} &= G_{\text{complex}} - G_{\text{protein}} - G_{\text{ligand}} \\ &= \Delta H + \Delta G_{\text{solvation}} - T\Delta S \\ &= \Delta E_{\text{MM}} + \Delta G_{\text{GB}} + \Delta G_{\text{SA}} - T\Delta S \end{aligned} \quad (1)$$

The binding free energy of GSK3 $\beta$  and inhibitors was calculated by MM/GBSA method. In this method, the struc-

**Table 2.** Statistical results of the CoMFA models.

	CoMFA(1)	CoMFA(2)	CoMFA(3)	CoMFA(4)	CoMFA(5)
$q^2$	0.594	0.157	0.510	0.359	0.267
$r^2$	0.975	0.630	0.938	0.978	0.964
SEE	0.189	0.670	0.290	0.177	0.220
F	140.347	18.108	71.819	160.441	128.241
Components	5	2	4	5	4
Steric	0.647	-	-	0.278	-
Electrostatic	0.353	-	-	0.230	-
Steric (indicator)	-	-	0.612	-	0.280
Electrostatic (indicator)	-	-	0.388	-	0.202
H-bond acceptor	-	0.605	-	0.340	0.350
H-bond donor	-	0.395	-	0.152	0.168
$R^2_{test}$	0.756	0.418	0.412	0.467	0.477
$^a$ RMSE	0.337	0.640	0.313	0.274	0.271

$$^a\text{RMSE (root mean-square error)} = \sqrt{\frac{\sum(Y_{pic50} - Y_{pred})^2}{n}}$$

ture of a frame system is extracted every 10 ps from the last 10 ns MD simulation trajectory of the composite for free energy calculation. Where  $\Delta G_{\text{complex}}$ ,  $\Delta G_{\text{protein}}$  and  $\Delta G_{\text{ligand}}$  are the free energies of the complex, protein and inhibitor respectively. The free energy of gas phase ( $\Delta E_{\text{MM}}$ ) can be divided into electrostatic free energy ( $\Delta G_{\text{ele}}$ ) and van der Waals free energy ( $\Delta G_{\text{vdw}}$ ), and the free energy of solvation ( $\Delta G_{\text{sol}}$ ) can be divided into polar solvent free energy ( $\Delta G_{\text{GB}}$ ) and non-polar solvent free energy ( $\Delta G_{\text{SA}}$ ). The contribution of polar solvent free energy to solvent free energy can be calculated by Generalized Born. In the calculation, the dielectric constant of solute and the permittivity of solvent are set to 1 and 80 respectively. The contact surface area of solvent was calculated by LCPO method.

The binding free energy was decomposed using the GBSA (Generalized Born/Surface Area) method, which decomposed the binding free energy of ligand-binding receptors into the contributions of the backbone atoms and side chain atoms of each residue. Equation (2) shows that proteins interact with small molecules in four different ways [17, 37, 40-45].

$$\Delta G_{\text{inhibitor-residue}} = \Delta E_{\text{vdw}} + \Delta G_{\text{ele}} + \Delta G_{\text{GB}} + \Delta G_{\text{SA}} \quad (2)$$

### 3. RESULTS AND DISCUSSION

#### 3.1. 3D-QSAR Results Analysis

##### 3.1.1. CoMFA Model Analysis

The CoMFA model based on superposition was used for the prediction of a series of pyrazine inhibitors in the following study. Five models based on the traditional (electrostatic and steric) fields and the ‘‘Advanced CoMFA’’ module containing H-bond fields and indicator fields were both investigated [46]. The results of these CoMFA models were summarized in Table 2. It is remarkable that CoMFA(1) and CoMFA(3) show better results than the other models, the  $q^2$  values are 0.594 and 0.510, respectively. And then, the bio-

activities of the compounds in the testing set were predicted by these models, and the predictive correlation coefficients ( $R^2_{test}$ ) were all calculated to evaluate the accuracies of these models. Meanwhile, the root mean-square error (RMSE) of all inhibitors were calculated, respectively. As shown in Table 2, although CoMFA(1) and CoMFA(3) both show satisfactory results ( $q^2 > 0.5$ ), CoMFA(1) contains the best predictive ability ( $R^2_{test} = 0.756$ ). Therefore, CoMFA(1) was chosen to the following analysis. The CoMFA(1) model demonstrated a  $q^2$  value of 0.594, with optimal principal of components 5. PLS analysis provided conventional  $r^2$  value of 0.975, SEE value of 0.189, and F value of 140.387, which indicated that the model contained a good predictive ability ( $q^2 > 0.5$  and  $r^2 > 0.9$ ). In CoMFA model, the contributions of steric and electrostatic fields were 64.7% and 35.3% respectively, it suggested that the steric field contributed most to the GSK3 $\beta$  inhibitory activity. In addition, the experimental PIC<sub>50</sub> and predicted PIC<sub>50</sub> of all inhibitors are shown in Table S1 and the predicted correlation coefficient ( $R^2$ ) between them are illustrated in Fig. (1a). ( $R^2_{training} = 0.975$  and  $R^2_{test} = 0.756$ ), these results suggested that the developed CoMFA model has a robust predictive capability for subsequent QSAR analysis.

##### 3.1.2. Analysis of CoMFA Model Contour Maps

The contour maps of CoMFA model can directly reflect the effects of steric and electrostatic field parameters on the activity of compounds, and further guide the rational design of compounds. In the contour maps of the steric field, the yellow area indicates that the introduction of larger groups will reduce the activity, while the green area indicates that the introduction of larger groups will increase the activity of compounds. While in the electrostatic field, the red region represents that the introduction of negative groups can improve the activity of compounds, and the blue region represents that the introduction of positive groups can improve the activity of compounds. In order to facilitate the analysis and

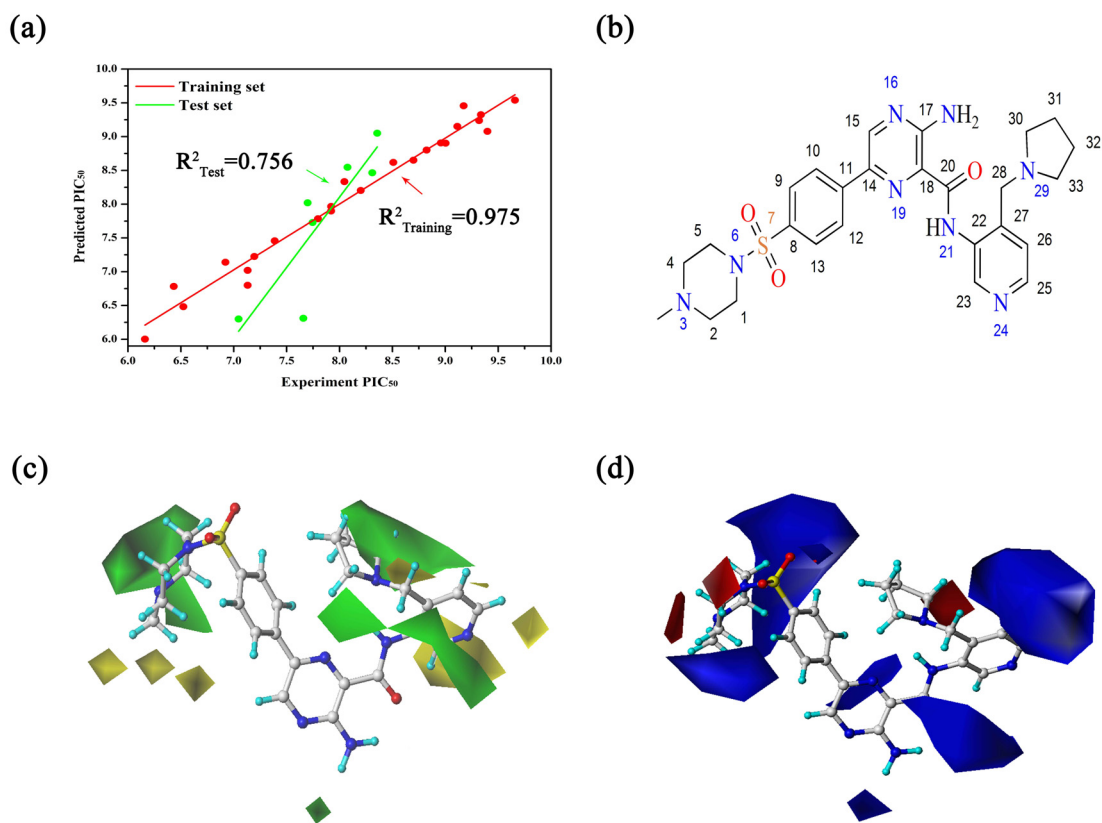


**Fig. (1).** (a) Plots of predicted PIC<sub>50</sub> values versus experimental PIC<sub>50</sub> values for the CoMFA models (training set colored in red and test set colored in green); (b) the structure of Cpd25; (c) steric contour maps; (d) electrostatic contour maps.

discussion of the CoMFA model equipotential diagram, Cpd25 (Fig. 1b), with the highest inhibitory activity, is displayed in the maps to aid in visualization.

The steric fields of CoMFA are shown in Fig. (1c), a large green contour was mapped near 3 and 4 positions of piperazine ring, indicating that this area was suitable for the introduction of bulky groups substituents. For example, Cpd18 (PIC<sub>50</sub> = 8.310) had a bulkier substituent (methylpiperazinyl group) at position 3, and that significantly increased the activity compared to Cpd8 (PIC<sub>50</sub> = 7.131) or Cpd9 (PIC<sub>50</sub> = 6.523). Similarly, one large green area in the 30<sup>th</sup> and 31<sup>st</sup> attachments suggest that the introduction of large volume substituents nearby has a great improvement in biological activity. For example, Cpd25 (PIC<sub>50</sub> = 9.658) has a higher activity than Cpd26 (PIC<sub>50</sub> = 9.319) because of the introduction of 4-pyrrolidin-2-ylpyridine group at R<sub>5</sub> substitution. Finally, although there is just a small green contour between the 16 and 17 sites, a bulky group still would improve the biological activity, like Cpd27 (PIC<sub>50</sub> = 6.921), along with the introduction of a polyatomic cycloalkyl group, showed higher inhibition than Cpd41 (PIC<sub>50</sub> = 6.432). On the contrary, three small yellow contours surrounding carbon terminal of the site 3 indicated that a bulky group at this position would decrease the potency. By checking the analogues, it could be observed that Cpd20 (PIC<sub>50</sub> = 9.398) had higher activity than Cpd18 (PIC<sub>50</sub> = 8.310) substituted with bulky methyl groups at 6-position. Meanwhile, there are several yellow areas around the 21-nitrogen-connected pyri-

dine, in the case of Cpd46 (PIC<sub>50</sub> = 9.004), the activity is significantly higher than that of Cpd44 (PIC<sub>50</sub> = 7.921), Cpd45 (PIC<sub>50</sub> = 6.161) and Cpd49 (PIC<sub>50</sub> = 7.131). The above statement also can be confirmed by Cpd25, due to the introduction of the large substituted cyclopentane in the green region at R<sub>5</sub> substituent (Table 1), the activity of Cpd25 was significantly improved.

The electrostatic fields of CoMFA is shown in Fig. (1d). one small red contour appears near 3 and 4 positions, suggested their affinity to electron-withdrawing substituents. If these positions were replaced by electron donating groups, it would result in a decrease of inhibitory activity. For example, when Cpd22 (PIC<sub>50</sub> = 9.174) introduced oxygen atoms at 3 positions, the biological activity increased by about 7 times compared with Cpd18 (PIC<sub>50</sub> = 8.310). By contrast, a large blue area was covered around the piperazine ring, indicating that the introduction of electropositive groups was a benefit to biological activity. For example, the activity of Cpd18 is significantly higher than that of Cpd21 (PIC<sub>50</sub> = 7.921), because N-methylpiperazinyl sulfonyl is more positive than sulfonamide. There are red region and larger blue region near position 7, suggesting that the area of electrical factors is more complex, which needs specific analysis. For Cpd25, position 8 was substituted by piperazine sulfonyl group, and it is clearly observed from Fig. (1d) that the electro negativity of sulfonyl is in the red areas, while the location of the piperazine ring in the blue area, observed to have increased activity. In addition, there is one small blue region between



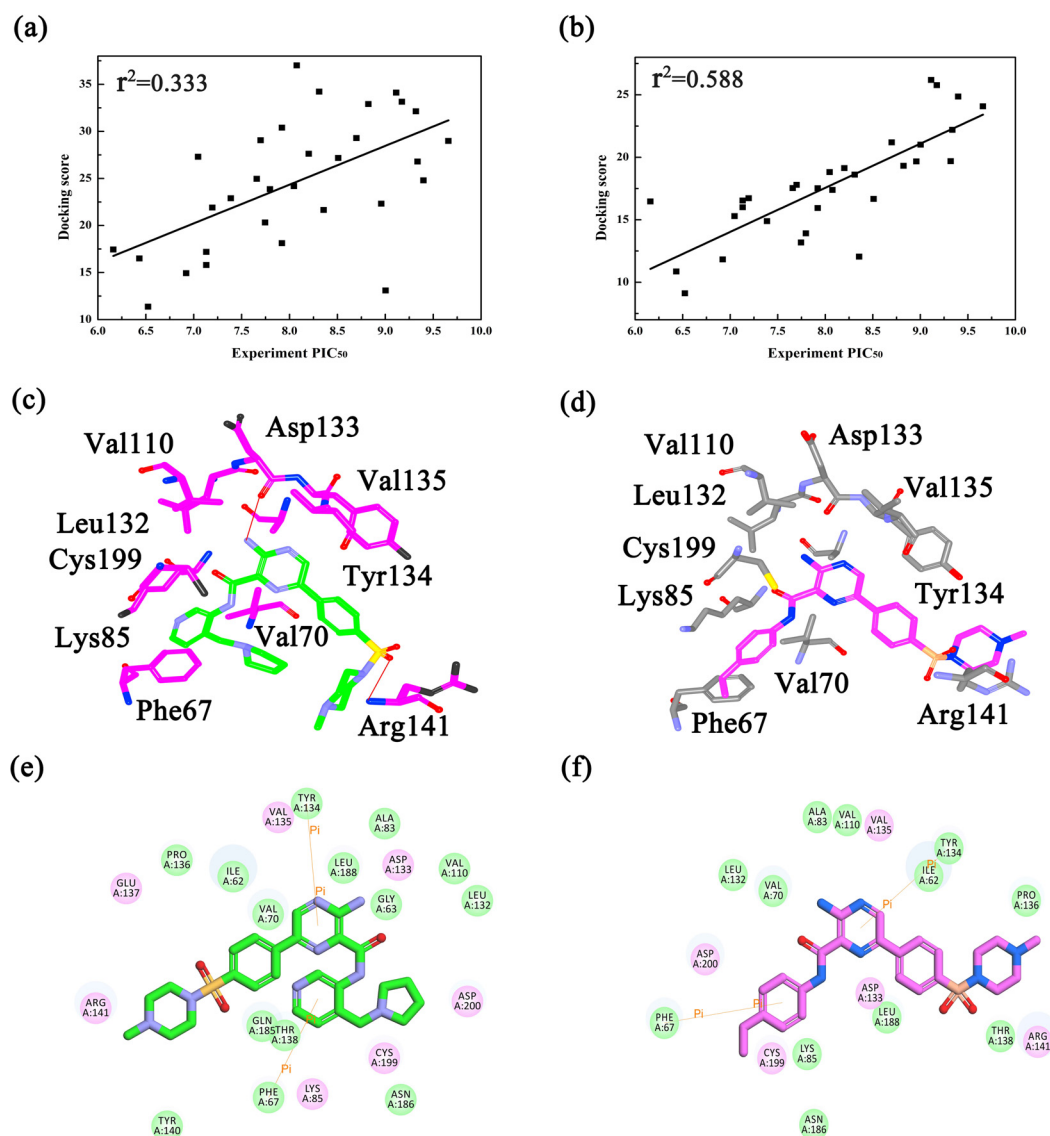


**Fig. (2).** (a) The correlations between the experimental  $PIC_{50}$  and the docking scores by (a) CDOCKER and (b) Flexible Docking; Flexible docking model of (c) Cpd25 and (d) Cpd45 in the active site of GSK3 $\beta$ ; 2D presentations of the interactions between GSK3 $\beta$  and (e) Cpd25; (f) Cpd45.

16 and 17 sites, which indicated that the introduction of a positive group in the vicinity was profitable to the enhancement of biological activity. For example, Cpd28 bearing electro-withdrawing groups at position 17 displayed distinct improvements in potency which compared with Cpd41. Between Cpd25 and 26 located the blue area, such as Cpd46 ( $PIC_{50} = 9.004$ ) whose activity was significantly higher than the Cpd49 ( $PIC_{50} = 7.131$ ).

## 3.2. Molecular Docking Analysis

### 3.2.1. Comparison of Two Docking Methods

Molecular docking studies are widely used as a method of predicting the potential binding mechanisms between the bio-active compound and the protein [17, 47]. Firstly, in order to investigate the “docking power” [48, 49] of all crystal structures of GSK3 $\beta$ , the ligands extracted from four crystal structures were re-docked into the corresponding GSK3 $\beta$  proteins.

And the RMSD (root mean square deviation) values between the re-docked complex and the initial crystal structure was calculated to compare. As illustrated in Fig. (S2a-d), the docking pose of Cpd18 superimposed onto the crystal structure better than the other complexes (RMSD = 0.93 Å, Fig. S2b), thus Cpd18 was selected to perform the next docking protocols. Secondly, to verify the accuracy of two docking protocols, the crystal structure of 4ACD coupled with Cpd18 was re-docked by FD, and as shown in Fig. (S2e), the FD docked pose of Cpd18 superimposed better (RMSD = 0.56 Å) than CD (RMSD = 0.93 Å), it implicated that FD would perform well for this system. On the other hand, the correlation coefficients ( $r^2$ ) of both docking protocols were evaluated to detect the relationship between the observed experimental values ( $PIC_{50}$ ) against the predicted docking scores of the protein-ligand complexes. As shown in Figs. (2a and b), the predicted scores obtained by FD show greater linear correlation ( $r^2 = 0.588$ ) than CD docking ( $r^2 = 0.333$ ), which means



the flexibility of protein is crucial for binding between GSK3 $\beta$  and the inhibitors. The overall results proved that FD more accurate than CD for the next analysis.

### 3.2.2. Analysis of Docking Results

Based on the above docking results, the discussion was mainly focused on the FD re-docked complexes. Fig. (S2f) shows the alignments of all docked structures in the binding site of GSK3 $\beta$ , and all the docked molecules share similar binding modes. In order to evaluate the effects of different molecular alignments on CoMFA model [50], the FD docking poses of all the inhibitors (Fig. S2f) were constructed using CoMFA models with different fields, and the results are summarized in Table S2. Some models showed the good  $q^2$  values, such as CoMFA (1) = 0.561, CoMFA(5) = 0.556, but it is disappointing that all of them exhibited poor predictive abilities (Table S2). Be that as it may, these docking poses still provide valuable information for exploring the structure-activity relationship between GSK3 $\beta$  and the inhibitors. In the case of Cpd25 and Cpd45 (Figs. 2c and d), the docking results revealed that Cpd25 and Cpd45 bound to the same position of GSK3 $\beta$  and the residues Phe67, Ala83, Lys85, Val110, Leu132, Asp133, Tyr134, Val135, Arg141, Cys199 constructed the ATP pocket almost surrounded by both inhibitors. Meanwhile, Fig. (2c) showed that Cpd25 formed two hydrogen bonds (H-bond) with Asp133 and Arg141, while these H-bonds lost between GSK3 $\beta$  and Cpd45, these H-bond interactions could keep strong affinity to GSK3 $\beta$  and that is consistent with the large difference of bioactivities between them. The pyridine ring and piperazine ring of Cpd25 and 45, respectively formed  $\pi$ - $\pi$  stacking and  $\pi$ -cation interactions with Phe67, Tyr134 (Figs. 2e and f). The above results indicate that the H-bonds and  $\pi$ -cation interactions play important roles in maintaining the stability of binding interactions between the ligand and GSK3 $\beta$  [17]. In addition, the structure of GSK3 $\beta$  minor changes adapts to different inhibitors. For example, compared with Cpd25 (Figs. 2e and f), when interacting with Cpd45, several residues, including Phe67, Val70, Asp133 and Arg141, showed major conformational changes to adapt the structure of Cpd45. This further shows the importance of the flexibility of GSK3 $\beta$  for inhibitor-target recognition.

## 3.3. Molecular Dynamics Simulation

### 3.3.1. Binding Free Energy Calculations

In order to evaluate the dynamic binding process of the studied inhibitors and rationality of the simulated complex system, the RMSD variation of the complex structure with

respect to the initial structure skeleton atoms during the simulation process was calculated and the results are shown in Fig. (S3). The plots showed that all studied systems reached equilibrium within 10 ns, with an average about 1.5Å RMSD fluctuation. Based on the MD simulations, to explore the most favorable binding mechanism of the studied complex, the binding free energies for the four inhibitors were calculated and the results are summarized in Table 3. Simultaneously, non-polarity bond was significantly stronger than that of the polarity bond of all the studied inhibitors. Van der Waals force and electrostatic terms are quite favorable for inhibitor binding to GSK3 $\beta$ , while the polar solvation term is unfavorable for binding in all four complexes. Non-polar contribution ( $\Delta_{vdw} + \Delta_{SA}$ ) of 4ACG/Cpd25 (-88.400 kcal $\cdot$ mol $^{-1}$ ) is significantly stronger than that of 4ACC/Cpd23 (-51.480 kcal $\cdot$ mol $^{-1}$ ), 4ACH/Cpd51 (-74.300 kcal $\cdot$ mol $^{-1}$ ) and 4ACM/Cpd23 (-54.020 kcal $\cdot$ mol $^{-1}$ ), which agreed with the GSK3 $\beta$  inhibitory activities assayed *in vitro*.

### 3.3.2. Analysis of the Inhibitors Binding Mechanism

For the sake of quantitatively identify the contribution of each residue to inhibitors, the total binding free energies for four complexes were further decomposed into individual residue contributions. The comparison of the inhibitor-residues energy difference is illustrated in Figs. (3, 4 and S4). As Fig. (3) appears at a first glance, all three complexes share several similar interaction patterns with the active site residues, such as Val70, Asp133, Tyr134, Val135, Arg141 of GSK3 $\beta$ , their contributions to  $\Delta G_{pred}$  are all lower than -2.0 kcal $\cdot$ mol $^{-1}$  (Figs. (3a-c), respectively). Obviously, the majority of these residues are all hydrophobic amino acids, that makes the non-polar interactions become the dominating force for the inhibitor binding. Meanwhile, some of the other residues that give rise to the difference in their bioactivities which are summarized in Figs. (3a-c), such as Ile62, Lys85. Then, in order to explore the detail effects of different substituents, the comparison of the inhibitor-receptor for three groups (4ACC/Cpd23 and 4ACG/Cpd25, 4ACH/Cpd51 and 4ACG/Cpd25, 4ACC/Cpd23 and 4ACM/Cpd23) were illustrated in Fig. (3).

Compared to Cpd23, modifications at two sites were found in Cpd25, the ethylene diamine group at the 6-position (Fig. 1b) in Cpd23 was replaced by N-methylpiperazinyl-sulfonyl group, and the hydrogen atom at the 28-position in Cpd23 was replaced by a methylpiperolidinyl group. These changes enhance the activity from 20 nM (Cpd23) to 0.220 nM (Cpd25). As illustrated in Table 3, the energy contribution of van der Waals interactions for Cpd25 is -57.400

**Table 3. MM/GBSA energy components and binding free energies ( $\Delta G_{pred}$ ) versus experimental data.**

Complex	$\Delta E_{vdw}$	$\Delta E_{ele}$	$\Delta G_{SA}$	$\Delta G_{GB}$	$\Delta G_{Pred}$	PIC <sub>50</sub>
4ACC/23	-47.19 $\pm$ 0.95	-34.43 $\pm$ 0.32	-4.29 $\pm$ 0.17	47.16 $\pm$ 0.57	-38.75 $\pm$ 0.02	7.699
4ACG/25	-57.40 $\pm$ 0.48	-31.00 $\pm$ 0.32	-5.00 $\pm$ 0.24	46.37 $\pm$ 0.33	-47.03 $\pm$ 0.12	9.658
4ACH/51	-48.84 $\pm$ 0.47	-25.46 $\pm$ 0.49	-4.39 $\pm$ 0.28	43.20 $\pm$ 0.44	-35.49 $\pm$ 0.01	7.658
4ACM/23	-49.65 $\pm$ 0.14	-29.14 $\pm$ 1.65	-4.37 $\pm$ 0.21	50.66 $\pm$ 0.29	-32.52 $\pm$ 0.46	7.432

kcal $\cdot$ mol $^{-1}$  and that for Cpd23 is  $-47.190$  kcal $\cdot$ mol $^{-1}$ , it shows that the van der Waals interactions are important for the inhibitors binding. Followed by Figs. (3a and b), it is easy to observe that Lys85 and Arg141 are significant for the interactions both Cpd23 and Cpd25. Meanwhile, the energy contribution of Lys85 for Cpd25 is  $-2.270$  kcal $\cdot$ mol $^{-1}$ , which is more favorable than that of Cpd23 ( $-1.610$  kcal $\cdot$ mol $^{-1}$ ), the Arg141 works in a similar way. The difference in the contributions of Lys85 and Arg141 for Cpd23 and Cpd25 is mainly caused by the strong van der Waals interactions, which leads to a closer contact between the sulfonyl group of Cpd25 and Arg141 than that the corresponding Lys85 of

Cpd23 (Fig. 3d). As displayed in Figs. (3a and b), both Cpd23 and Cpd25 formed favorable interactions with Tyr134. However, the energy contribution of Tyr134 in the 4ACC/Cpd23 complex ( $-1.870$  kcal $\cdot$ mol $^{-1}$ ) is lower than that in the 4ACG/Cpd25 complex ( $-2.590$  kcal $\cdot$ mol $^{-1}$ ). Tyr134 formed hydrophobic interaction with Cpd25, while that interaction lost in Cpd23 system. According to the previous molecular docking analysis, pyridine ring formed the key H-bond interactions with residue Lys85 in the GSK3 $\beta$  active site. Therefore, Lys85 is a critical residue for inhibitor binding to GSK3 $\beta$ .

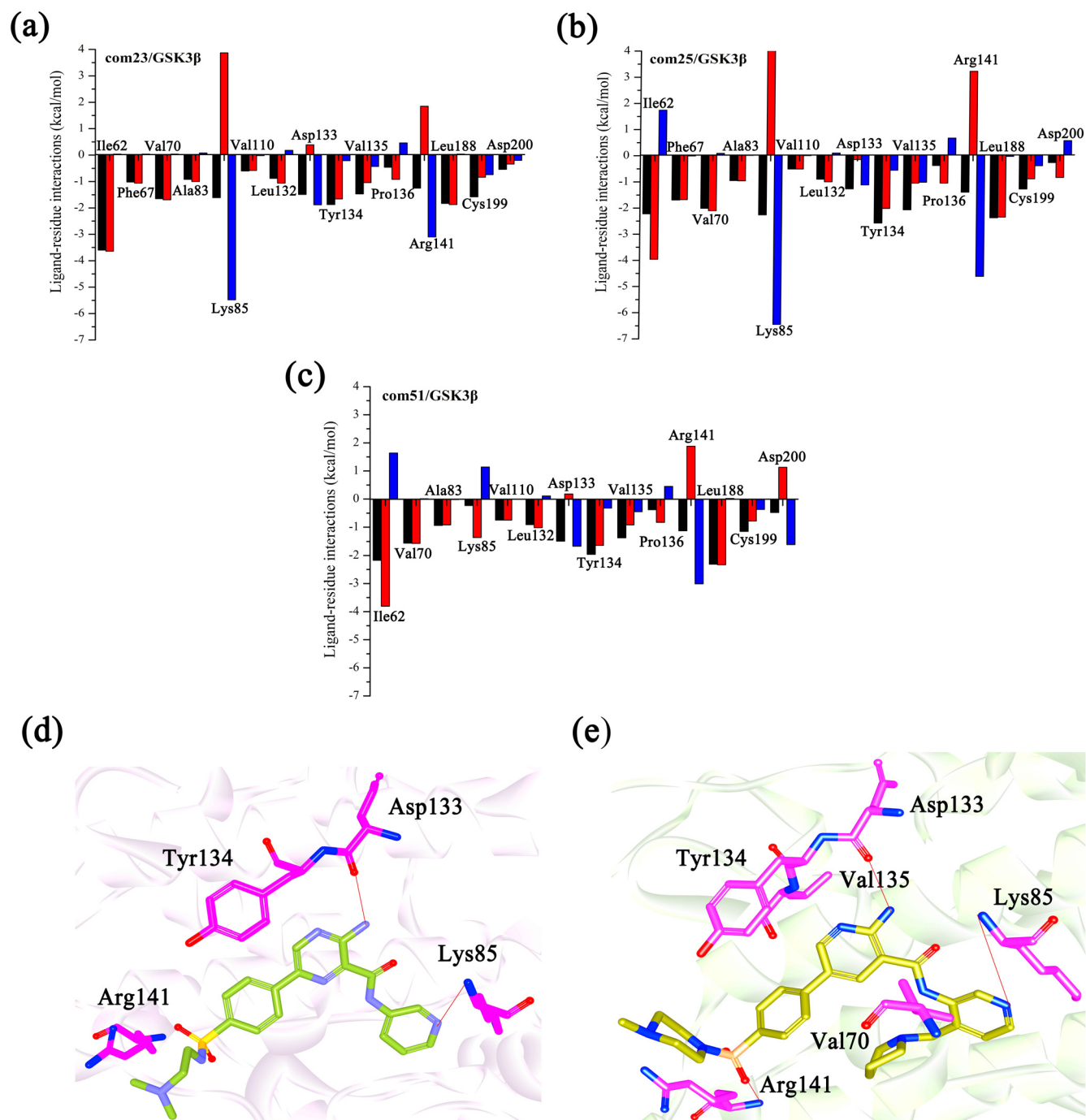
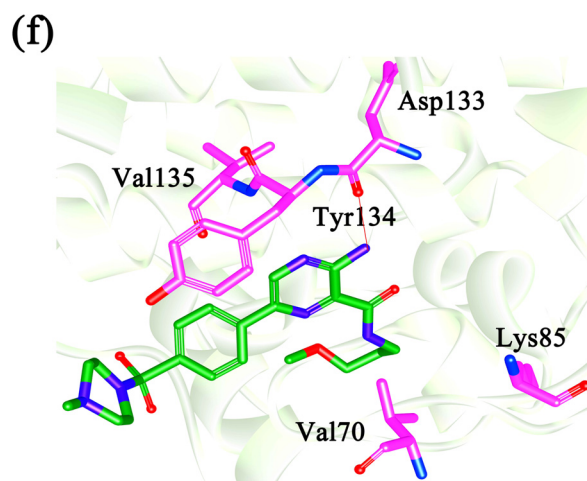


Fig. (3). Contd...



**Fig. (3).** The changes of inhibitor-residue spectrum for (a) GSK3 $\beta$ /Cpd23; (b) GSK3 $\beta$ /Cpd25; (c) the GSK3 $\beta$ /Cpd51 (The black columns represent the total binding free energy, the red columns represent the non-polar energy ( $\Delta_{vdw} + \Delta_{SA}$ ) and the blue columns represent the polar energy ( $\Delta_{ele} + \Delta_{GB}$ ); the binding mode of (d) GSK3 $\beta$ /Cpd23; (e) GSK3 $\beta$ /Cpd25; (f) GSK3 $\beta$ /Cpd51.

Besides, Cpd51 also was chosen to compare with Cpd25. The difference of structure between Cpd25 and Cpd51 just lie in the groups at the 22-position (Fig. 1b). Cpd25 contained a 4-pyrrolidin-2-ylpyridine group at 22-position while Cpd51 had a methyl propyl ether group (Table 1). However, Cpd25 showed better inhibitory activity ( $IC_{50} = 0.220$  nM) than Cpd51 ( $IC_{50} = 22$  nM). The reason for the difference mainly depends on the various contributions formed by several key residues, including Lys85, Tyr134 and Val135. The modification at the 22-position enhanced the inhibitors interaction with the residue Lys85. The energy difference of Val134 between Cpd25 and Cpd51 is  $0.630$  kcal $\cdot$ mol $^{-1}$  (Fig. 3b and c), and it is primarily contributed from the differences between the van der Waals interactions ( $-2.450$  kcal $\cdot$ mol $^{-1}$  and  $-2.080$  kcal $\cdot$ mol $^{-1}$ , respectively). As illustrated in Figs. (3c and d), the 2-Phenylpiperazine group in Cpd25 and Cpd51 was close to Val134 and therefore they both formed strong interactions with Val134. The interactions between the inhibitors and Tyr135 are similar to the above discussion. However, Val70 share more favorable contributions to the binding affinity of Cpd25 than that of Cpd51. This can also be explained by the position of the pyrrolidine of Cpd25 in Fig. (3e). Overall, we can draw the conclusion that a large group at the 22-position would enhance the ligand-protein interactions, which is consistent with 3D-QSAR result discussed above.

In addition, to explore the selectivity mechanism between GSK3 $\beta$  and CDK2, two complexes 4ACC and 4ACM, containing the same inhibitor (Cpd23) were investigated. Table 3 showed that predicted binding free energy for 4ACC/Cpd23 is weaker than that for 4ACM/Cpd23, suggesting that Cpd23 formed stronger interactions with GSK3 $\beta$  than CDK2, which is consistent with the experimental data. To better understand the distinction in the binding affinity between 4ACC/Cpd23 and 4ACM/Cpd23, the data from the binding energy decomposition analysis also should be considered. According to Figs. (4a-c), the residues Ile62/Ile10, Val70/Val18, Ala83/Ala31, Leu132/Phe80, Tyr134/Phe82, Leu188/Leu134, share strong contributions to the interactions between GSK3 $\beta$  and CDK2. It is interesting to observe that all these important residues are hydrophobic, which all

can form strong van der Waals interactions with the inhibitors. Among these residues, Ile62/Ile10 are more essential to determine the difference in the binding affinity of both two complexes. The van der Waals interaction between Cpd23 and Ile62 ( $-3.160$  kcal $\cdot$ mol $^{-1}$ ) is more favorable than that between Cpd23 and Ile10 ( $-2.390$  kcal $\cdot$ mol $^{-1}$ ). The enhanced van der Waals interactions between Ile62/Ile10 and Cpd23 are mainly caused by the change position of the 2-(dimethylaminoethyl)-ethylamino. Besides, the Cpd23 can form H-bonds with the Asp133 and Arg141 of GSK3 $\beta$  and the H-bonds also could be observed between Cpd23 and Glu81 and Asp86 of CDK2. But the H-bond formed by Asp133 of GSK3 $\beta$  ( $-1.500$  kcal $\cdot$ mol $^{-1}$ ) stronger than that of Glu81/CDK2 ( $-0.590$  kcal $\cdot$ mol $^{-1}$ ). Meanwhile, both of the polar and non-polar interactions between Cpd23 and Arg141 ( $-1.260$  kcal $\cdot$ mol $^{-1}$ ) are stronger than those between Cpd23 and Asp86 ( $-0.380$  kcal $\cdot$ mol $^{-1}$ ). Overall, Ile62/Ile10, Asp133/Glu81 and Arg141/Asp86 are more essential to determine the difference of the binding affinity of both complexes. In a word, Ile62, Asp133, Arg141 may be the key residues for GSK3 $\beta$  selectivity inhibition.

## CONCLUSION

In this work, a computational analysis, integrating 3D-QSAR, molecular docking and molecular dynamics simulation was conducted to explore the specific binding mechanisms of GSK3 $\beta$  ATP competition inhibitors. The CoMFA model with high linear correlation  $R^2_{Pred}$  provides reliable predictive ability and the three-dimensional isopotential maps delicately revealed the structure-activity relationships. The results of molecular docking show that the introduction of the flexibility of GSK3 $\beta$  may significantly improve the accuracy of prediction and FD provides appropriate binding modes of the inhibitors. And then, MD simulations were performed to deeply understand the dynamic binding mode between GSK3 $\beta$ /ligand complexes and some key residues for improving the affinities to GSK3 $\beta$  were identified. At last, the inhibitor specificity between GSK3 $\beta$  and CDK2 is determined by the additive contributions of multiple amino acids, such as Ile62, Asp133 and Arg141. In conclusion, all

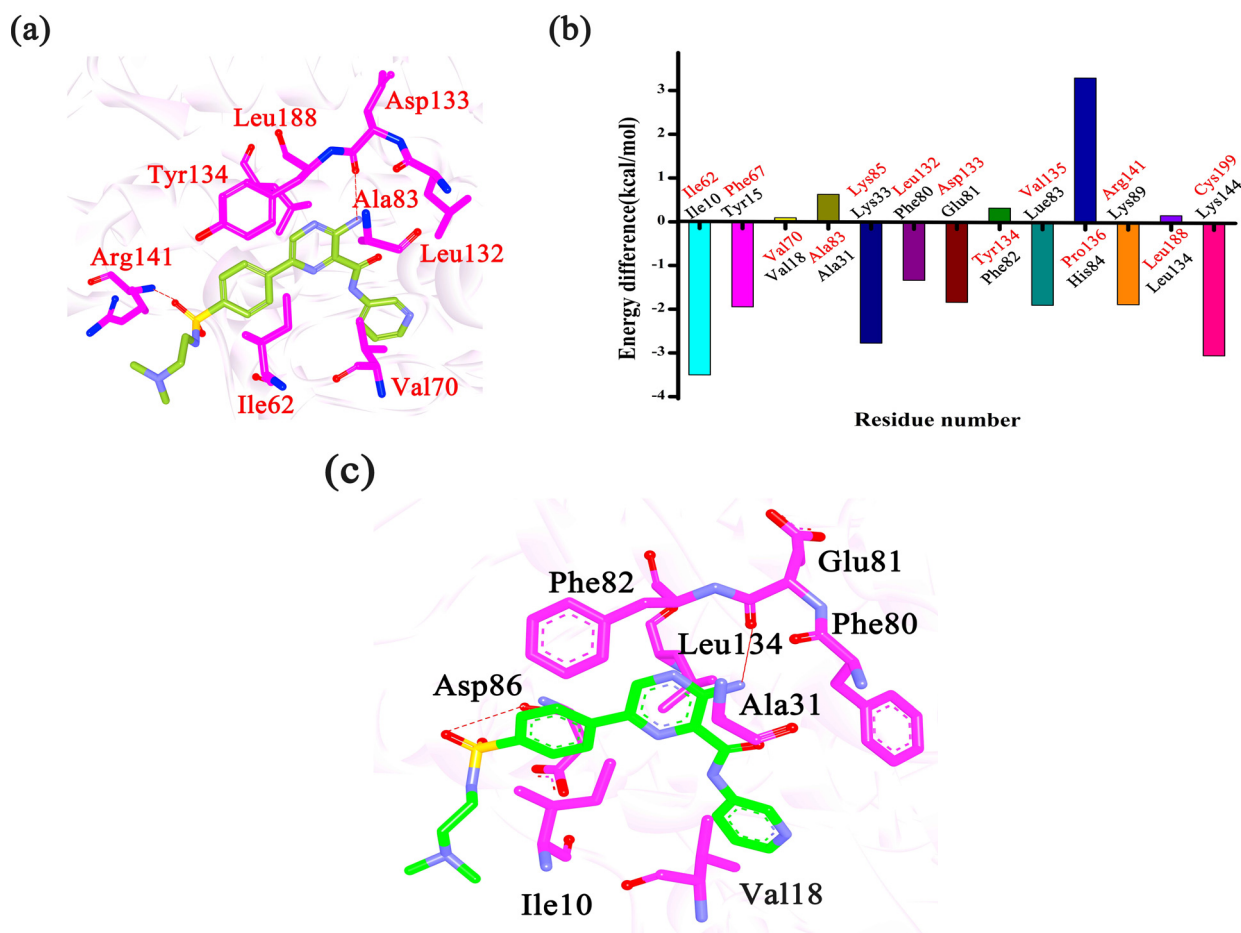


**Fig. (4).** (a) The binding mode of GSK3 $\beta$ /Cpd23; (b) the negative value of ( $\Delta_{vdw} + \Delta_{ele}$ ) represents a favorable contribution for GSK3 $\beta$  and the positive value of ( $\Delta_{vdw} + \Delta_{ele}$ ) represents a favorable contribution for CDK2; (c) the binding mode of CDK2/Cpd23.

the above results provide useful information to understand the mechanism of inhibitor binding and specificity and may provide useful information for the rational design of novel and selective GSK3 $\beta$  ATP competition inhibitors.

#### ETHICS APPROVAL AND CONSENT TO PARTICIPATE

Not applicable.

#### HUMAN AND ANIMAL RIGHTS

No Animals/Humans were used for studies that are the basis of this research.

#### CONSENT FOR PUBLICATION

Not applicable.

#### AVAILABILITY OF DATA AND MATERIALS

The data that support the findings of this study are available from the corresponding author, [Jingyu Zhu], upon reasonable request.

#### FUNDING

None.

#### CONFLICT OF INTEREST

The authors declare no conflict of interest, financial or otherwise.

#### ACKNOWLEDGEMENTS

Declared none.

#### SUPPLEMENTARY MATERIAL

Supplementary material is available on the publisher's website along with the published article.

#### REFERENCES

- [1] Hu, X.L.; Guo, C.; Hou, J.Q.; Feng, J.H.; Zhang, X.Q.; Xiong, F.; Ye, W.C.; Wang, H. Stereoisomers of Schisandrin B are potent ATP competitive GSK-3 $\beta$  inhibitors with neuroprotective effects against Alzheimer's disease: Stereochemistry and biological activity. *ACS Chem. Neurosci.*, **2019**, *10*(2), 996-1007. [<http://dx.doi.org/10.1021/acscchemneuro.8b00252>] [PMID: 29944335]
- [2] Frame, S.; Cohen, P. GSK3 takes centre stage more than 20 years after its discovery. *Biochem. J.*, **2001**, *359*(Pt 1), 1-16. [<http://dx.doi.org/10.1042/bj3590001>] [PMID: 11563964]
- [3] Pandey, M.K.; DeGrado, T.R. Glycogen synthase kinase-3 (GSK-3)-targeted therapy and imaging. *Theranostics*, **2016**, *6*(4), 571-593.

- [4] [http://dx.doi.org/10.7150/thno.14334] [PMID: 26941849]  
Cohen, P.; Frame, S. The renaissance of GSK3. *Nat. Rev. Mol. Cell Biol.*, **2001**, 2(10), 769-776.
- [5] [http://dx.doi.org/10.1038/35096075] [PMID: 11584304]  
Diehl, J.A.; Cheng, M.; Roussel, M.F.; Sherr, C.J. Glycogen synthase kinase-3beta regulates cyclin D1 proteolysis and subcellular localization. *Genes Dev.*, **1998**, 12(22), 3499-3511.
- [6] [http://dx.doi.org/10.1101/gad.12.22.3499] [PMID: 9832503]  
Zhang, M.; Zhang, P.; Liu, Y.; Zhou, Y. GSK3 inhibitor AR-A014418 promotes osteogenic differentiation of human adipose-derived stem cells via ERK and mTORC2/Akt signaling pathway. *Biochem. Biophys. Res. Commun.*, **2017**, 490(2), 182-188.
- [7] [http://dx.doi.org/10.1016/j.bbrc.2017.06.018] [PMID: 28602697]  
Maqbool, M.; Hoda, N. GSK3 inhibitors in the therapeutic development of diabetes, cancer and neurodegeneration: Past, present and future. *Curr. Pharm. Des.*, **2017**, 23(29), 4332-4350.
- [8] [http://dx.doi.org/10.2174/1381612823666170714141450] [PMID: 28714403]  
Abdul, A.U.R.M.; De Silva, B.; Gary, R.K. The GSK3 kinase inhibitor lithium produces unexpected hyperphosphorylation of  $\beta$ -catenin, a GSK3 substrate, in human glioblastoma cells. *Biol. Open*, **2018**, 7(1)bio030874.
- [9] [http://dx.doi.org/10.1242/bio.030874] [PMID: 29212798]  
Cohen, P.; Goedert, M. GSK3 inhibitors: Development and therapeutic potential. *Nat. Rev. Drug Discov.*, **2004**, 3(6), 479-487.
- [10] [http://dx.doi.org/10.1038/nrd1415] [PMID: 15173837]  
Penas, C.; Mishra, J.K.; Wood, S.D.; Schürer, S.C.; Roush, W.R.; Ayad, N.G. GSK3 inhibitors stabilize Wee1 and reduce cerebellar granule cell progenitor proliferation. *Cell Cycle*, **2015**, 14(3), 417-424.
- [11] [http://dx.doi.org/10.4161/15384101.2014.974439] [PMID: 25616418]  
Force, T.; Woodgett, J.R. Unique and overlapping functions of GSK-3 isoforms in cell differentiation and proliferation and cardiovascular development. *J. Biol. Chem.*, **2009**, 284(15), 9643-9647.
- [12] [http://dx.doi.org/10.1074/jbc.R800077200] [PMID: 19064989]  
Dey, A.; Hao, S.; Wosiski-Kuhn, M.; Stranahan, A.M. Glucocorticoid-mediated activation of GSK3 $\beta$  promotes tau phosphorylation and impairs memory in type 2 diabetes. *Neurobiol. Aging*, **2017**, 57, 75-83.
- [13] [http://dx.doi.org/10.1016/j.neurobiolaging.2017.05.010] [PMID: 28609678]  
Swinney, Z.T.; Haubrich, B.A.; Xia, S.; Ramesha, C.; Gomez, S.R.; Guyett, P.; Mensa-Wilmot, K.; Swinney, D.C. A four-point screening method for assessing molecular mechanism of action (MMOA) identifies tideglusib as a time-dependent inhibitor of trypanosoma brucei GSK3beta. *PLoS Negl. Trop. Dis.*, **2016**, 10(3), e0004506
- [14] [http://dx.doi.org/10.1371/journal.pntd.0004506] [PMID: 26942720]  
Saura, C.; Roda, D.; Roselló, S.; Oliveira, M.; Macarulla, T.; Pérez-Fidalgo, J.A.; Morales-Barrera, R.; Sanchis-García, J.M.; Musib, L.; Budha, N.; Zhu, J.; Nannini, M.; Chan, W.Y.; Sanabria Bohórquez, S.M.; Meng, R.D.; Lin, K.; Yan, Y.; Patel, P.; Baselga, J.; Taberner, J.; Cervantes, A. A first-in-human phase I study of the ATP-competitive AKT inhibitor ipatasertib demonstrates robust and safe targeting of AKT in patients with solid tumors. *Cancer Discov.*, **2017**, 7(1), 102-113.
- [15] [http://dx.doi.org/10.1158/2159-8290.CD-16-0512] [PMID: 27872130]  
Wagman, A.S.; Johnson, K.W.; Bussiere, D.E. Discovery and development of GSK3 inhibitors for the treatment of type 2 diabetes. *Curr. Pharm. Des.*, **2004**, 10(10), 1105-1137.
- [16] [http://dx.doi.org/10.2174/1381612043452668] [PMID: 15078145]  
Martinez, A.; Castro, A.; Dorronsoro, I.; Alonso, M. Glycogen synthase kinase 3 (GSK-3) inhibitors as new promising drugs for diabetes, neurodegeneration, cancer, and inflammation. *Med. Res. Rev.*, **2002**, 22(4), 373-384.
- [17] [http://dx.doi.org/10.1002/med.10011] [PMID: 12111750]  
Zhao, S.; Zhu, J.; Xu, L.; Jin, J. Theoretical studies on the selective mechanisms of GSK3 $\beta$  and CDK2 by molecular dynamics simulations and free energy calculations. *Chem. Biol. Drug Des.*, **2017**, 89(6), 846-855.
- [18] [http://dx.doi.org/10.1111/cbdd.12907] [PMID: 27863047]  
Arfeen, M.; Bharatam, P.V. Design of glycogen synthase kinase-3 inhibitors: An overview on recent advancements. *Curr. Pharm. Des.*, **2013**, 19(26), 4755-4775.
- [19] [http://dx.doi.org/10.2174/1381612811319260007] [PMID: 23260024]  
García, I.; Fall, Y.; Gómez, G. QSAR, docking, and CoMFA studies of GSK3 inhibitors. *Curr. Pharm. Des.*, **2010**, 16(24), 2666-2675.
- [20] [http://dx.doi.org/10.2174/138161210792389225] [PMID: 20642432]  
Patil, R.; Sawant, S. Molecular dynamics guided receptor independent 4D QSAR studies of substituted coumarins as anticancer agents. *Curr Comput Aided Drug Des*, **2015**, 11(1), 39-50.
- [21] [http://dx.doi.org/10.2174/1573409911666150617113933] [PMID: 26081557]  
Yang, Y.; Qin, J.; Liu, H.; Yao, X. Molecular dynamics simulation, free energy calculation and structure-based 3D-QSAR studies of B-RAF kinase inhibitors. *J. Chem. Inf. Model.*, **2011**, 51(3), 680-692.
- [22] [http://dx.doi.org/10.1021/ci100427j] [PMID: 21338122]  
Yu, H.; Fang, Y.; Lu, X.; Liu, Y.; Zhang, H. Combined 3D-QSAR, molecular docking, molecular dynamics simulation, and binding free energy calculation studies on the 5-hydroxy-2H-pyridazin-3-one derivatives as HCV NS5B polymerase inhibitors. *Chem. Biol. Drug Des.*, **2014**, 83(1), 89-105.
- [23] [http://dx.doi.org/10.1111/cbdd.12203] [PMID: 23941500]  
Balasubramanian, P.K.; Balupuri, A.; Kang, H.Y.; Cho, S.J. Receptor-guided 3D-QSAR studies, molecular dynamics simulation and free energy calculations of Btk kinase inhibitors. *BMC Syst. Biol.*, **2017**, 11(Suppl. 2), 6.
- [24] [http://dx.doi.org/10.1186/s12918-017-0385-5] [PMID: 28361711]  
Chaudhari, H.K.; Pahelkar, A.R. 3D QSAR, docking, molecular dynamics simulations and MM-GBSA studies of extended side chain of the antitubercular drug (6S) 2-Nitro-6-{[4-(trifluoromethoxy) benzyl] oxy}-6,7-dihydro-5H-imidazo[2,1-b][1,3] oxazine. *Infect. Dis. Drug Tar.*, **2018**.
- [25] [http://dx.doi.org/10.1002/minf.201400045] [PMID: 27486081]  
Fu, G.; Liu, S.; Nan, X.; Dale, O.R.; Zhao, Z.; Chen, Y.; Wilkins, D.E.; Manly, S.P.; Cutler, S.J.; Doerksen, R.J. Quantitative structure-activity relationship analysis and a combined ligand-based/structure-based virtual screening study for Glycogen Synthase Kinase-3. *Mol. Inform.*, **2014**, 33(9), 627-640.
- [26] [http://dx.doi.org/10.1111/j.1747-0285.2011.01291.x] [PMID: 22168279]  
Akhtar, M.; Bharatam, P.V. 3D-QSAR and molecular docking studies on 3-anilino-4-arylmaleimide derivatives as glycogen synthase kinase-3 $\beta$  inhibitors. *Chem. Biol. Drug Des.*, **2012**, 79(4), 560-571.
- [27] [http://dx.doi.org/10.1007/s11030-013-9483-5] [PMID: 24081608]  
Quesada-Romero, L.; Caballero, J. Docking and quantitative structure-activity relationship of oxadiazole derivatives as inhibitors of GSK3 $\beta$ . *Mol. Divers.*, **2014**, 18(1), 149-159.
- [28] [http://dx.doi.org/10.1007/s11030-013-9483-5] [PMID: 24081608]  
Berg, S.; Bergh, M.; Hellberg, S.; Högdin, K.; Lo-Alfredsson, Y.; Söderman, P.; von Berg, S.; Weigelt, T.; Örmö, M.; Xue, Y.; Tucker, J.; Neelissen, J.; Jerning, E.; Nilsson, Y.; Bhat, R. Discovery of novel potent and highly selective glycogen synthase kinase-3 $\beta$  (GSK3 $\beta$ ) inhibitors for Alzheimer's disease: design, synthesis, and characterization of pyrazines. *J. Med. Chem.*, **2012**, 55(21), 9107-9119.
- [29] [http://dx.doi.org/10.1021/jm201724m] [PMID: 22489897]  
Case, D.A.; Cheatham, T.E., III; Darden, T.; Gohlke, H.; Luo, R.; Merz, K.M., Jr; Onufriev, A.; Simmerling, C.; Wang, B.; Woods, R.J. The Amber biomolecular simulation programs. *J. Comput. Chem.*, **2005**, 26(16), 1668-1688.
- [30] [http://dx.doi.org/10.1002/jcc.20290] [PMID: 16200636]  
Wang, J.; Wolf, R.M.; Caldwell, J.W.; Kollman, P.A.; Case, D.A. Development and testing of a general amber force field. *J. Comput. Chem.*, **2004**, 25(9), 1157-1174.
- [31] [http://dx.doi.org/10.1002/jcc.20035] [PMID: 15116359]  
Duan, Y.; Wu, C.; Chowdhury, S.; Lee, M.C.; Xiong, G.; Zhang, W.; Yang, R.; Cieplak, P.; Luo, R.; Lee, T.; Caldwell, J.; Wang, J.; Kollman, P. A point-charge force field for molecular mechanics simulations of proteins based on condensed-phase quantum mechanical calculations. *J. Comput. Chem.*, **2003**, 24(16), 1999-2012.
- [32] [http://dx.doi.org/10.1002/jcc.10349] [PMID: 14531054]  
Pedersen, M.; Klarlund, M.; Jacobsen, S.; Svendsen, A.J.; Frisch, M. Validity of rheumatoid arthritis diagnoses in the Danish National Patient Registry. *Eur. J. Epidemiol.*, **2004**, 19(12), 1097-1103.
- [32] [http://dx.doi.org/10.1007/s10654-004-1025-0] [PMID: 15678789]



- [33] Pan, P.; Yu, H.; Liu, Q.; Kong, X.; Chen, H.; Chen, J.; Liu, Q.; Li, D.; Kang, Y.; Sun, H.; Zhou, W.; Tian, S.; Cui, S.; Zhu, F.; Li, Y.; Huang, Y.; Hou, T. Combating drug-resistant mutants of anaplastic lymphoma kinase with potent and selective type-I(1/2) inhibitors by stabilizing unique DFG-shifted loop conformation. *ACS Cent. Sci.*, **2017**, *3*(11), 1208-1220. [http://dx.doi.org/10.1021/acscentsci.7b00419] [PMID: 29202023]
- [34] Sun, H.; Duan, L.; Chen, F.; Liu, H.; Wang, Z.; Pan, P.; Zhu, F.; Zhang, J.Z.H.; Hou, T. Assessing the performance of MM/PBSA and MM/GBSA methods. 7. Entropy effects on the performance of end-point binding free energy calculation approaches. *Phys. Chem. Chem. Phys.*, **2018**, *20*(21), 14450-14460. [http://dx.doi.org/10.1039/C7CP07623A] [PMID: 29785435]
- [35] Zhu, J.; Li, K.; Xu, L.; Jin, J. Insight into the selective mechanism of phosphoinositide 3-kinase gamma with benzothiazole and thiazolopiperidine gamma-specific inhibitors by *in silico* approaches. *Chem. Biol. Drug Des.*, **2018**. [PMID: 30582283]
- [36] Hou, T.; Wang, J.; Li, Y.; Wang, W. Assessing the performance of the MM/PBSA and MM/GBSA methods. 1. The accuracy of binding free energy calculations based on molecular dynamics simulations. *J. Chem. Inf. Model.*, **2011**, *51*(1), 69-82. [http://dx.doi.org/10.1021/ci100275a] [PMID: 21117705]
- [37] Gohlke, H.; Kiel, C.; Case, D.A. Insights into protein-protein binding by binding free energy calculation and free energy decomposition for the Ras-Raf and Ras-RalGDS complexes. *J. Mol. Biol.*, **2003**, *330*(4), 891-913. [http://dx.doi.org/10.1016/S0022-2836(03)00610-7] [PMID: 12850155]
- [38] Hou, T.; Li, Y.; Wang, W. Prediction of peptides binding to the PKA RIalpha subunit using a hierarchical strategy. *Bioinformatics*, **2011**, *27*(13), 1814-1821. [http://dx.doi.org/10.1093/bioinformatics/btr294] [PMID: 21586518]
- [39] Sun, H.; Li, Y.; Shen, M.; Tian, S.; Xu, L.; Pan, P.; Guan, Y.; Hou, T. Assessing the performance of MM/PBSA and MM/GBSA methods. 5. Improved docking performance using high solute dielectric constant MM/GBSA and MM/PBSA rescoring. *Phys. Chem. Chem. Phys.*, **2014**, *16*(40), 22035-22045. [http://dx.doi.org/10.1039/C4CP03179B] [PMID: 25205360]
- [40] Chen, F.; Sun, H.; Wang, J.; Zhu, F.; Liu, H.; Wang, Z.; Lei, T.; Li, Y.; Hou, T. Assessing the performance of MM/PBSA and MM/GBSA methods. Predicting binding free energies and poses of protein-RNA complexes. *RNA*, **2018**, *24*(9), 1183-1194. [http://dx.doi.org/10.1261/rna.065896.118] [PMID: 29930024]
- [41] Zhang, C.; Hou, T.; Feng, Z.; Li, Y. Structure-based development of antagonists for chemokine receptor CXCR4. *Curr Comput Aided Drug Des*, **2013**, *9*(1), 60-75. [http://dx.doi.org/10.2174/1573409911309010006] [PMID: 22734712]
- [42] Xu, L.; Kong, R.; Zhu, J.; Sun, H.; Chang, S. Unraveling the conformational determinants of LARP7 and 7SK small nuclear RNA by theoretical approaches. *Mol. Biosyst.*, **2016**, *12*(8), 2613-2621. [http://dx.doi.org/10.1039/C6MB00252H] [PMID: 27301448]
- [43] Liu, N.; Zhou, W.; Guo, Y.; Wang, J.; Fu, W.; Sun, H.; Li, D.; Duan, M.; Hou, T. Molecular dynamics simulations revealed the regulation of ligands to the interactions between androgen receptor and its coactivator. *J. Chem. Inf. Model.*, **2018**, *58*(8), 1652-1661. [http://dx.doi.org/10.1021/acs.jcim.8b00283] [PMID: 29993249]
- [44] Shen, M.; Zhou, S.; Li, Y.; Li, D.; Hou, T. Theoretical study on the interaction of pyrrolopyrimidine derivatives as LIMK2 inhibitors: Insight into structure-based inhibitor design. *Mol. Biosyst.*, **2013**, *9*(10), 2435-2446. [http://dx.doi.org/10.1039/c3mb70168a] [PMID: 23881296]
- [45] Shen, M.; Zhou, S.; Li, Y.; Pan, P.; Zhang, L.; Hou, T. Discovery and optimization of triazine derivatives as ROCK1 inhibitors: Molecular docking, molecular dynamics simulations and free energy calculations. *Mol. Biosyst.*, **2013**, *9*(3), 361-374. [http://dx.doi.org/10.1039/c2mb25408e] [PMID: 23340525]
- [46] Zhu, J.; Li, Y.; Yu, H.; Zhang, L.; Mao, X.; Hou, T. Insight into the structural requirements of narpaprevir-type inhibitors of NS3/NS4A protease based on HQSAR and molecular field analyses. *Comb. Chem. High Throughput Screen.*, **2012**, *15*(6), 439-450. [http://dx.doi.org/10.2174/138620712800563918] [PMID: 22263860]
- [47] Zhu, J.; Pan, P.; Li, Y.; Wang, M.; Li, D.; Cao, B.; Mao, X.; Hou, T. Theoretical studies on beta and delta isoform-specific binding mechanisms of phosphoinositide 3-kinase inhibitors. *Mol. Biosyst.*, **2014**, *10*(3), 454-466. [http://dx.doi.org/10.1039/C3MB70314B] [PMID: 24336903]
- [48] Tian, S.; Sun, H.; Pan, P.; Li, D.; Zhen, X.; Li, Y.; Hou, T. Assessing an ensemble docking-based virtual screening strategy for kinase targets by considering protein flexibility. *J. Chem. Inf. Model.*, **2014**, *54*(10), 2664-2679. [http://dx.doi.org/10.1021/ci500414b] [PMID: 25233367]
- [49] Tian, S.; Sun, H.; Li, Y.; Pan, P.; Li, D.; Hou, T. Development and evaluation of an integrated virtual screening strategy by combining molecular docking and pharmacophore searching based on multiple protein structures. *J. Chem. Inf. Model.*, **2013**, *53*(10), 2743-2756. [http://dx.doi.org/10.1021/ci400382r] [PMID: 24010823]
- [50] AbdulHameed, M.D.; Hamza, A.; Liu, J.; Zhan, C.G. Combined 3D-QSAR modeling and molecular docking study on indolinone derivatives as inhibitors of 3-phosphoinositide-dependent protein kinase-1. *J. Chem. Inf. Model.*, **2008**, *48*(9), 1760-1772. [http://dx.doi.org/10.1021/ci800147v] [PMID: 18717540]